SUPPLEMENTAL MATERIAL

"Nonlocal detection of out-of-plane magnetization in a magnetic insulator by thermal spin drag"

Can Onur Avci[1,2], Ethan Rosenberg[1], Mantao Huang[1], Jackson Bauer[1], Caroline A. Ross[1], Geoffrey S.D. Beach[1]

[1]*Department of Materials Science and Engineering, Massachusetts Institute of Technology, Cambridge, Massachusetts 02139, USA*

[2]*Department of Materials, ETH Zürich, CH-8093 Zürich, Switzerland*

SM.1 Absence of spin current injection to TmIG by the TaOx/Au heater layer

We performed control experiments on Au/TaOx strips by injecting 20 mA of ac current and measuring the longitudinal first (R_{ω}) and second harmonic ($R_{2\omega}$) resistance. As evident from Fig. SM1, we could not detect any magnetically relevant signals in the first harmonic (spin Hall magnetoresistance) and second harmonic (spin Seebeck effect) channels of the longitudinal resistance. These results confirm our assumption that there is no spin current flowing from Au to the TmIG which could give rise to long range magnon transport.

SM.2 – Control measurements with double heater channels

To verify the in-plane gradient dependence of the SNMR and spin drag signals, and to find out the gradient responsible for the SSE signals, we have fabricated a sample with the heater line on the opposite side of the Pt detector channel with equal separation d = 15 μm. Please note that the TmIG used in this experiment showed perpendicular magnetic anisotropy. Figure SM2 shows the device layout, electrical connections (a-c) and the data corresponding to the out-of-plane field sweep and in-plane angle scan measurements for the three cases of heat source [current through the bottom heater only (a), both heaters (b) and the top heater only (c)]. As evident from the data, we are able to control the sign of both thermal spin drag [(d) and (f)] and the spin Nernst magnetoresistance [(g) and (i)] signals, confirming that both effects exclusively depend on ∇T_{IP}. Note that in the data shown through the bottom row (g-i) the dashed and dotted lines show the decomposition of the raw data into the spin Seebeck effect ($\cos\varphi$) and spin Nernst magnetoresistance

($\sin 2\varphi$) contributions, respectively, based on the fitting function given in the main text ($V_{2\omega} = V_{\text{sse}}\nabla T_{OP}\cos\varphi + V_{\text{snmr}}\nabla T_{IP}\sin 2\varphi$). We also observed that the ∇T_{IP}-related signals completely vanish when the heating current was sent through both the channels [(e) and (h)], simultaneously, canceling out the net ∇T_{IP}. However, the spin Seebeck effect signal depends on ∇T_{OP} whose direction does not change by sending current through the opposite channels separately or both heater channels together. Therefore, these control experiments undoubtedly confirm all of our proposed temperature gradient scenarios and the signals associated with them.

SM.3 - Determination of device temperature profiles through resistivity measurements

We quantified the current-induced temperature rise of the heater and the detector channels by performing controlled temperature/heater current versus resistance experiments, which allowed us to measure the in-plane temperature gradient (∇T_{IP}) in our devices. We first mounted the sample on a thermoelectric plate and measured the resistance of heater and detector wires in two-point probe mode as a function of substrate temperature [Fig. SM3 (a)]. We found a linear increase in the resistance for both Au and Pt as a function of temperature as expected from the resistivity vs. T of elemental metals. We then measured the resistance as a function of d.c. current injection through the heater and detector channels and found that both resistances increase linearly as a function of I^2 [Fig.SM3 (b)], as expected from the standard Joule heating scenario ($T \propto I^2R$). We have then used these two measurements to find the relative change in the wire temperatures (ΔT) for both Au heater and Pt detector channel at various distances *d* as a function of current injected through the Au heater wire [Fig. SM3(c)]. We see that ΔT is significant in the heater wire and goes up to ~75°C (considering room temperature as 21°C) for a current of 28 mA. We note that for the harmonic measurements we have used an a.c. current and this value corresponds to I_{ac} = 40 mA (peak-to-peak), which is close to the maximum current we used, i.e., I_{ac} = 55 mA. Surprisingly, we also measured a non-negligible ΔT in the Pt detectors even though no current is flowing through them. Moreover, ΔT in the detector wires depends on their distance from the heater wire, indicating that there is an in-plane temperature gradient. To quantify the temperature gradient we plot ΔT for the heater and a series of detector wires in Fig. SM3 (d).

We observe that for all current values there is an exponential decay of ΔT. We use a simple exponential function ($\propto e^{-\beta d}$, with β= 1/decay length) to fit the data (black curves). Finally, by taking the derivative of the fitted curves with respect to d we obtain the temperature gradient at any given point away from the Au heater wire for each injected current value, as shown in Fig. SM4. We find that the gradient varies between 0 and 1 °C/μm depending on the distance from the heater wire. These set of measurements unequivocally show the presence of an in-plane temperature gradient in our devices and its quantitative estimate.

By using the data in Fig. SM4 we can estimate the amount of spin polarization in Pt for a given device and heater current. For the data in Fig. 4 (c) (d = 30 μm and I_{ac} = 50 mA) we estimate ∇T_{IP} ~ 0.5 K/μm. By taking into account the room temperature Seebeck coefficient of Pt (S_{Pt} = -5 μV/K) we can find the electric field in Pt parallel to the gradient as $E_l = S_{Pt} \nabla T_{IP} = 2.5$ V/m. If the free electrons in Pt were fully spin polarized, the transverse electric field (along the detector channel) could be obtained by $E_{t,max} = E_l \cdot \theta_{SN}$, where θ_{SN} is the spin Nernst angle of Pt. By taking $\theta_{SN} = 0.1$ as a reasonable estimate we obtain $E_{t,max} = 0.25$ V/m if the spin polarization in Pt were 100%. In Fig.4 (c) the voltage along the detector channel is found as 60 nV converting itself into $E_t = 0.0003$ V/m. By taking the ratio of $E_t/E_{t,max}$ we can estimate the spin polarization in Pt as 0.12% in this measurement. It is worth emphasizing that, additional to the transport properties of Pt, this value depends on many other factors such as the spin Seebeck coefficient of TmIG, the spin mixing conductance of TmIG/Pt interface and ∇T_{OP}.

Figures

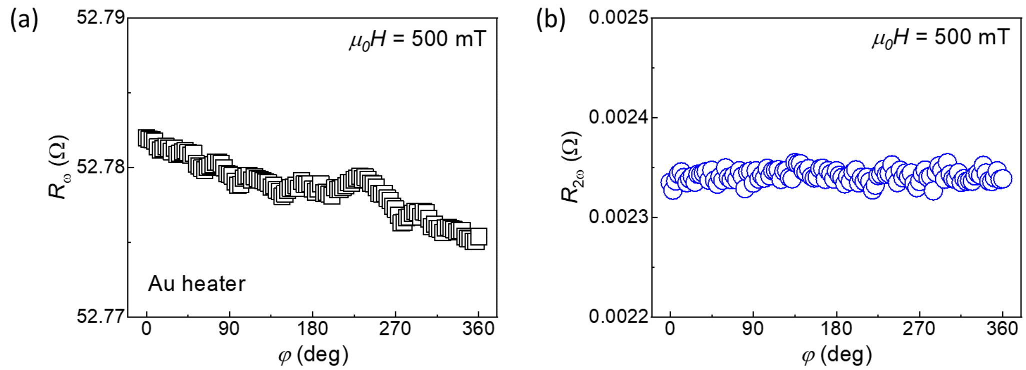

Figure SM1 – The first (a) and second harmonic (b) longitudinal resistance measured along the Au heater channel in four-point geometry. The sample is rotated on the x-y plane in the presence of a constant magnetic field of 500 mT. Note that the variations in (a) are due to thermal drift and are not reproducible, thereby do not represent any magnetization-related process.

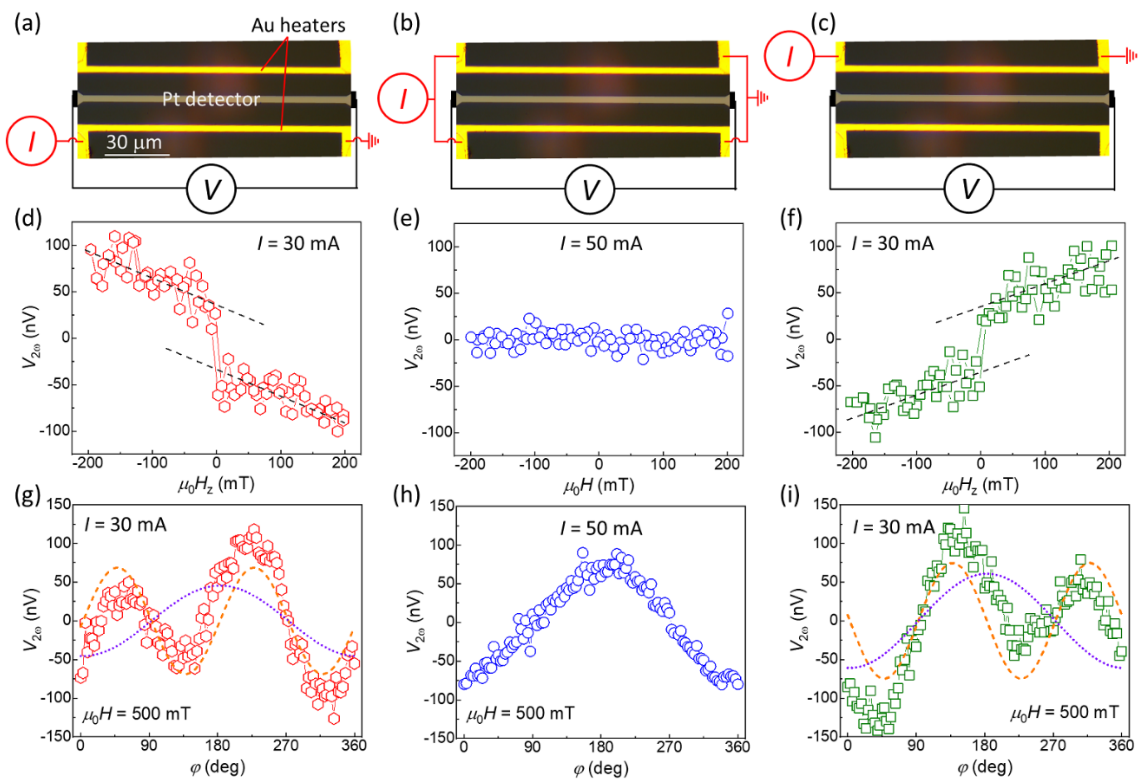

Figure SM2 – Experiments with double heater channels. (a-c) device micrograph and the electrical connections. The dark areas are TmIG. (d-e) Measuremets corresponding to the out-of-plane field sweep for respective heater current injection scenario. Clear jumps are observed around the zero field in (d) and (f) due to the

thermal spin drag mechanism upon magnetization reversal TmIG. (g-i) Measurements corresponding to the in-plane angle scan of a fixed external field of 500 mT. The sign is decomposed in the spin Nernst magnetoresistance (orange dashed line) and spin Seebeck effect (violet dotted line) contributions.

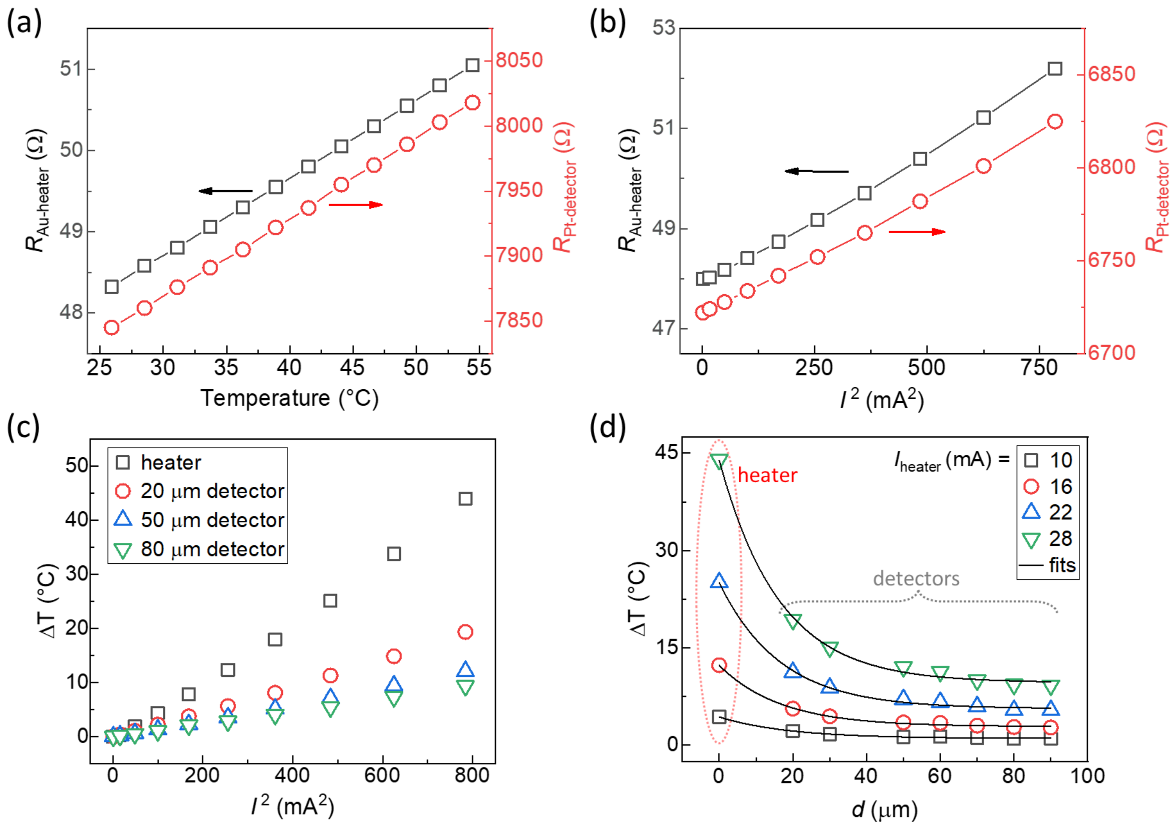

Figure SM3 – (a) Measurements of heater (left y-axis) and detector (right y-axis) channel resistances as a function of substrate temperature. (b) Measurements of heater (left y-axis) and detector (right y-axis) resistances as a function of current injected through their respective channels. Note that the heater-detector pair used in this experiment was different that that used for (a). The differences in resistance values are due mostly to the lithographic variations in the detector channel width. (c) Estimation of temperature rise in heater and detector channels upon current injection through the heater channel. (d) Estimation of temperature rise for the heather and detector channels as a function of *d* for different heater currents.

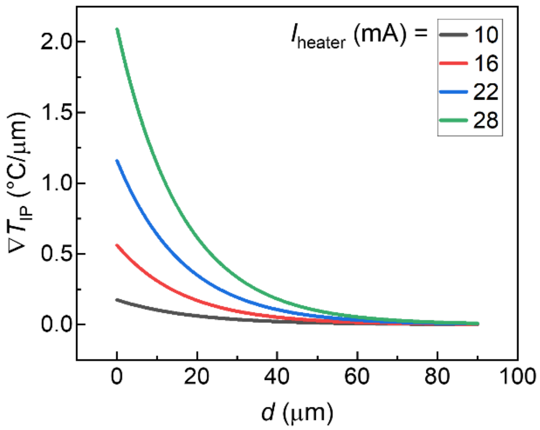

Figure SM4 – Estimated temperature gradients for different heater currents as a function of *d*.